Hypoxia and Inflammation-Induced Disruptions of the Blood-Brain and Blood-Cerebrospinal Fluid Barriers Assessed Using a Novel T_1-Based MRI Method

Nabeela Nathoo, Hamza Jalal, Sirajedin S. Natah, Qiong Zhang, Ying Wu, and Jeff F. Dunn

Introduction

The blood-brain barrier (BBB) protects the brain from potentially harmful elements circulating in the body. Disruption of the BBB is implicated in many neurological conditions, including stroke [1, 2], epilepsy [3, 4], and radiation-induced necrosis [5]. Such BBB disruption can be classified as being either severe or subtle. Severe BBB disruption can be discerned qualitatively as it is localized to specific areas of the brain, and can be assessed by determining the permeability of large molecular weight molecules such as serum proteins [6]. Severe disruption has been demonstrated radiologically with contrast agent extravasation in stroke [7, 8], traumatic brain injury [9, 10], and brain tumors [11].

Subtle disruption is found generalized throughout the brain, which requires quantitative methods for assessment. Methods include using smaller molecular weight compounds such as sodium fluorescein (NaF) or Evans blue [12], which are useful in histological studies but not in whole brain studies. Such subtle BBB disruption may be involved in multiple sclerosis [13] and high-altitude hypoxia exposure [14].

To study BBB disruption that is diffuse and relatively small in magnitude *in vivo*, an MRI method with increased sensitivity to the extravasation of the gadolinium (Gd) contrast agent is needed. Ideally, this method would detect leakage within a single voxel of an image. We propose a single voxel analysis and use models of severe and focal disruption contrast with mild and generalized disruption of the BBB to show proof of principle.

Severe disruption is based on the cold injury model, which generates a localized region of cortical injury and BBB disruption. Hypoxia leads to nonspecific and diffuse disruptions of the BBB, which has been previously demonstrated with enhancement on NaF histology [14]. We also compared this with an established model of lipopolysaccharide (LPS)-associated inflammatory generalized disruption.

Thus, we developed a novel voxel-based analysis facilitating visualization of BBB disruption at the level of a single voxel. This approach would provide the opportunity to quantify diffuse BBB disruption without having to select an arbitrary region of interest (ROI). Using this technique, we propose that mild hypoxia and inflammation resulted in diffuse disruption of the BBB, while more severe insults resulted in prominent leakage in the periventricular area.

Materials and Methods

Animals

Male Wistar rats were used (220–275 g) from Charles River (Montreal, Quebec). Studies were approved by the Animal Care Committee of the University of Calgary.

[AU1] N. Nathoo • H. Jalal
[AU2] Department of Radiology, University of Calgary, 3330 Hospital Drive, N.W., Calgary, AB T2N 4N1, Canada

Hotchkiss Brain Institute, University of Calgary, Calgary, AB Canada

S.S. Natah
Department of Physiology, Umm-Alqura University, Makkah, Saudi Arabia

Q. Zhang
General Electric, Beijing, China

Y. Wu
Department of Radiology, University of Calgary, 3330 Hospital Drive, N.W., Calgary, AB T2N 4N1, Canada

J.F. Dunn (✉)
Hotchkiss Brain Institute, University of Calgary, Calgary, AB Canada

Experimental Imaging Centre, University of Calgary, Calgary, AB Canada

Department of Radiology, University of Calgary, 3330 Hospital Drive, N.W., Calgary, AB T2N 4N1, Canada
e-mail: dunnj@ucalgary.ca

R.L. Applegate et al. (eds.), *Brain Edema XVI: Translate Basic Science into Clinical Practice*, Acta Neurochirurgica Supplement, Vol. 121,
DOI 10.1007/978-3-319-18497-5_5,

Cold Injury Model

This method has been described previously [15]. Two rats were anesthetized with 1–2 % isoflurane anesthesia. At approximately 3 mm posterior to the bregma and 2 mm lateral, a 2.5 mm hole was drilled, exposing the dura mater. Using forceps, the dura was removed, exposing the underlying brain. A metal probe (2 mm) cooled in liquid nitrogen for 5 min was applied to the surface for 45 s. For the sham rat, the same probe at room temperature was applied. The scalp was sutured and the animals were given a subcutaneous injection of analgesic (Buprenex; 0.3 mg/kg). Magnetic resonance imaging (MRI) was performed 24 h later.

LPS Treatment

Intraperitoneal (IP) injection was given at 0.1 or 1.0 mg/kg ($n=5$ for each concentration). With this model, increased BBB permeability occurs after 3–6 h [16]. MRI was performed 3 h later.

Hypoxia

For hypobaric (10 %) hypoxia, rats ($n=5$) were placed in a custom-built hypobaric chamber [14] and exposed for 24 h at 375 mmHg and 22 °C, which corresponded to a PO_2 of 78.8 mmHg. For more severe hypoxia (8 %), rats ($n=2$) were placed in a normobaric chamber with an O_2:N_2 (8:92 %) gas mixture, corresponding to PO_2 of 60.8 mmHg. After 24 h, rats were removed from the hypoxic chamber and transported to the imaging center (within 5 min) and administered an O_2:N_2 gas mixture with an equivalent FiO_2 to match the hypobaric chamber PO_2. Animals were anesthetized with 3 % isoflurane for MRI.

MRI Protocol

A 9.4T Bruker Avance console was used with a 35 mm quadrature volume coil. A cannula was placed intravenously for delivery of Gd (Gd; gadodiamide [Omniscan, GE Healthcare, USA]; 0.5 mmol/kg body weight). Hypobaric hypoxia rats were given O_2:N_2 of 10:88.5 %, normobaric hypoxia rats an 8:90.5 % mixture, and control animals were given a 30:68.5 % gas mixture with 1.5 % isoflurane. Body temperature was measured and maintained at 37 °C.

In two animals, Gd was injected in the magnet and a time course study was done to determine how much time needed to pass in order for the signal to reach steady state and to collect the second set of images. After determining this, Gd was injected and T_1-weighted spin echo images were acquired (TR = 500 ms, TE = 6 ms, matrix = 256 × 256, number of averages = 2, FOV = 3 × 3 cm, slice thickness = 1.5 mm).

NaF Histology

After MRI and while sedated, animals were given 1.0 mL of sodium fluorescein (2 % NaF (w/v) in normal saline 0.9 %; Sigma) intravenously. After 10 min, the animal was injected with ketamine (intraperitoneally; 1 mL/kg), and perfusion fixed with saline and 4 % paraformaldehyde. Brains were extracted and stored at 4 °C until sectioning, at which time brains were frozen in the cryostat for 30 min at −20 °C. Cryostat sections were cut at 50 µm and imaged using a fluorescent microscope (Olympus BX61). Analysis was done using StereoInvestigator (MBF Bioscience, Williston, VT, USA).

Voxel-Based Analysis

Average signal intensity from the same voxel in a series of 6 pre-Gd, T_1-weighted standard spin echo images was compared with a series of 10 post-Gd images using a custom MATLAB code. Images were aligned to ensure co-registration of voxels. Absolute values of signal intensity (16-bit) were used for processing to eliminate automatic normalization and scaling effects by the software. The average signal intensity of the pre-Gd and post-Gd series of voxels was compared using the one-tailed Z-test. A map of probability values of obtaining the observed mean difference in intensities was created for each voxel.

Bonferroni's correction for multiple comparisons was used. A range of p-values were tested. The resultant p-value of 5×10^{-4} was used as the significance level for individual comparisons of voxels. Following statistical testing, voxels that were significantly enhanced ($p<5\times10^{-4}$) post-Gd appeared white.

Results

Validation of Voxel-Based Analysis Using Cold-Injury Model

Following induction of the cold-injury model, enhancement was qualitatively observed in the area of injury with Gd (Fig. 1a). This enhancement corresponded to the voxel-map

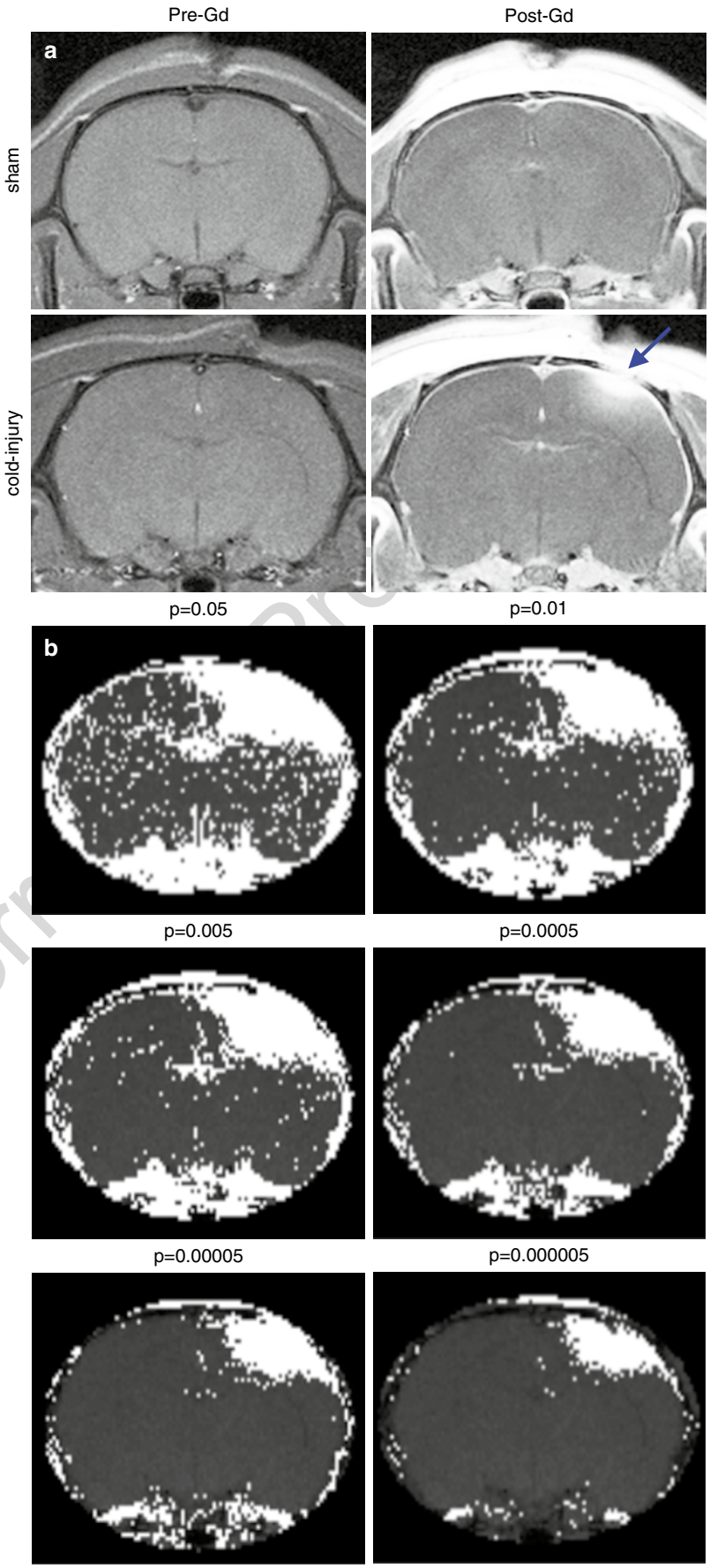

Fig. 1 Selection of significance value for voxel enhancement maps using T_1-weighted spin echo brain MRIs in the cold-injury model. Significantly enhanced voxels after Gd administration appear white. (**a**) Representative pre- and post-Gd T_1-weighted images for a sham rat and a cold injury rat. Area of injury in the cold injury model appears hyperintense post-Gd (*blue arrow*). (**b**) Signal intensities for post-Gd images were compared voxel-by-voxel using the *Z*-test with Bonferroni's correction for multiple comparisons. The effect of testing for statistical significance at different probability values based on the number of voxels included in the multiple comparisons is shown. Groups of 100 voxels were selected for statistical comparisons based on a qualitative analysis of background noise and phantoms resulting in significance inferred for changes in signal intensities of voxels at $p < 0.0005$

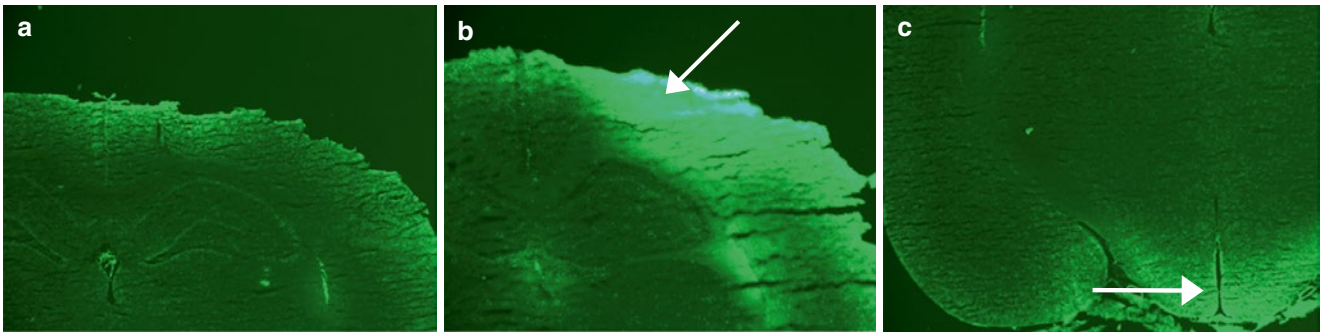

Fig. 2 Representative sodium fluorescein (NaF) histology for sham and cold-injury rats. (**a**) NaF histology for a sham rat with no obvious enhancement. (**b**) NaF histology for a rat that underwent cold injury. Intense focal enhancement is seen at the surgery site and adjacent area (*white arrow*). (**c**) NaF histology of a sham rat showing visible enhancement near the median eminence of the hypothalamus (area of weak BBB) (*white arrow*); this was seen for both conditions

that shows that significantly different voxels are clustered around the site of surgery and the surrounding area (Fig. 1b). A p-value of 5×10^{-4} was selected. Voxels that were significantly enhanced post-Gd appeared white.

NaF Histology for Cold-Injury Model

In sham animals, NaF enhancement was not observed at the surgery site (Fig. 2a). In cold injury animals, NaF enhancement was observed in the region surrounding the site of surgery (Fig. 2b); no enhancement was observed on the contralateral side. The median eminence, a circumventricular organ with a weak BBB, showed NaF enhancement in both sham and cold-injury animals (Fig. 2c).

Voxel-Based Analysis Shows Diffuse BBB Disruption in Low-Dose LPS and Mild Hypoxia

In control (Fig. 3a), low-dose LPS (Fig. 3b), and hypobaric hypoxia animals (Fig. 3d), no obvious areas of enhancement were observed. Furthermore, ROIs were drawn in the cortex, corpus callosum, and thalamus, and numbers of significant voxels were compared with controls. There was no significant difference ($p > 0.05$, one-way ANOVA with Dunnett's test post hoc). The third ventricle, however, showed significant enhancement; the fraction of significant voxels in the hypoxia group was 0.11 ± 0.01, while controls was 0.08 ± 0.01 (mean ± SEM).

Voxel-Based Analysis Shows Enhancement of the Periventricular Area in High-Dose LPS and Severe Hypoxia

In high-dose LPS animals, two responses were observed (Fig. 3c). The first was seen in two animals and consisted of significant periventricular disruption ($p < 0.0005$, Z-test) accompanied by enhancement throughout the parenchyma. The second was seen in the other three animals, where there was no obvious disruption of the BBB. Thus, it appears that once a threshold has been reached, the BBB becomes disrupted throughout the brain with a focus on leakage in the periventricular area.

Rats exposed to 8 % normobaric hypoxia also showed significant enhancement in the ventricles and periventricular area ($p < 0.0005$, Z-test) (Fig. 3e). Furthermore, there were increased numbers of individual voxels showing Gd enhancement throughout the parenchyma in severe hypoxia.

Discussion

It is fairly straightforward to detect major localized BBB disruption such as that in tumors or stroke with Gd-enhanced MRI [17]. Such disruptions cause enough T_1 signal change that regions can be seen without image processing. More quantitative methods, such as modeling the time course of enhancement or quantifying T_1, lead to voxel-based data that, theoretically, can be used to detect changes in a single voxel. However, these methods require modeling assumptions, and it may be difficult to identify changes within one voxel with a high degree of statistical confidence.

The method proposed here does not include a modeling assumption. The main statistical limitation is that the high number of comparisons made in a single test can lead to a type 1 error (differences are detected when none exist). To minimize this problem, we examined BBB disruption in a cold-injury model where we knew there would be significant focal disruption. When using a probability threshold often used in biological studies (i.e., $p < 0.05$), most of the brain showed significant change. This may, in part, be due to the fact that the blood T_1 was being shortened throughout the brain. The final p-value was selected to result in a statistical map that closely mapped the disruption observed using

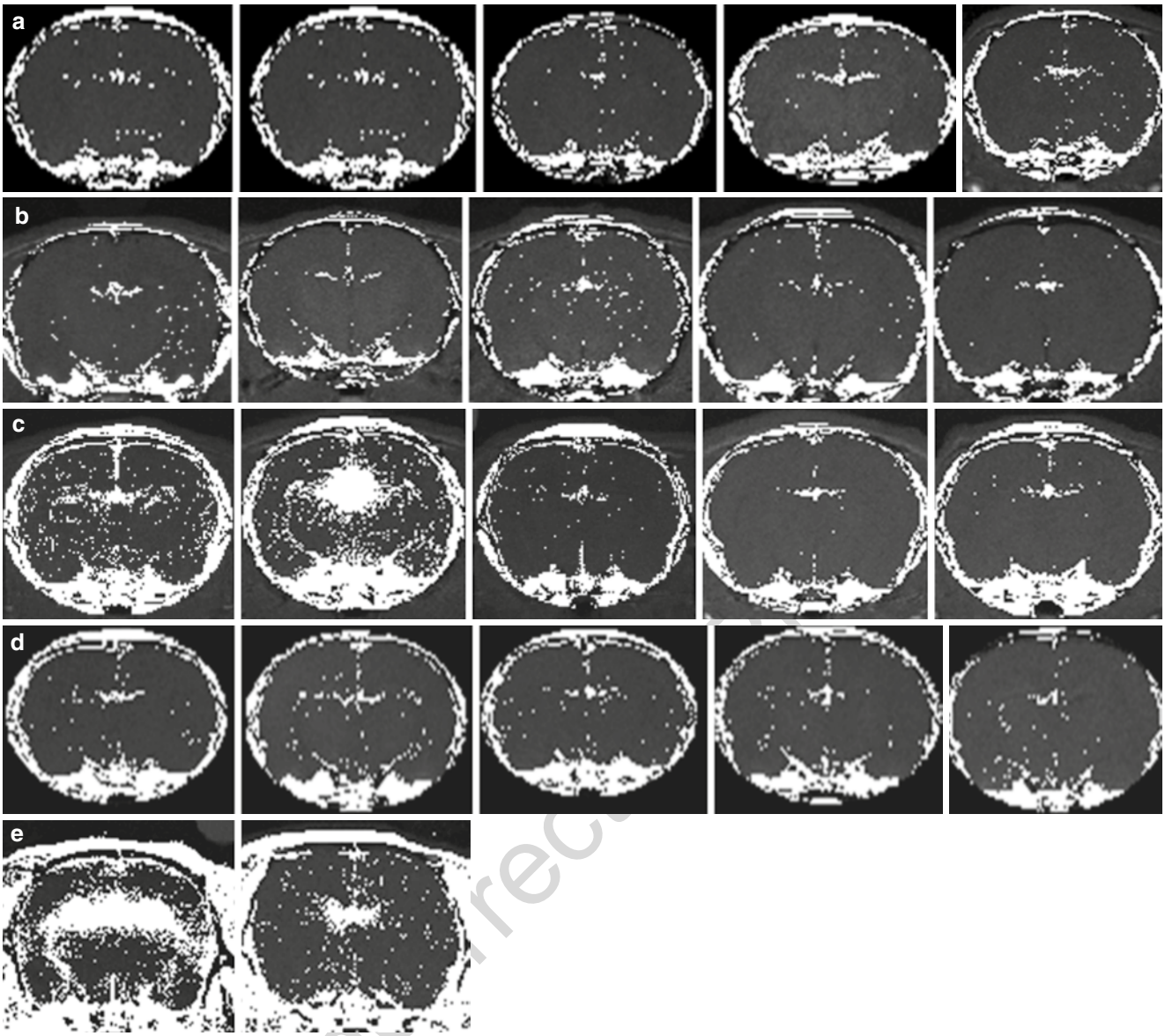

Fig. 3 Voxel-based analysis identified major enhancement in the periventricular area in the brains of rats exposed to high-dose lipopolysaccharide (LPS) and normobaric hypoxic conditions. Voxels with statistically increased signal after Gd administration are hyperintense. (**a**) Control rats that were exposed to 21 % O_2. (**b**) Rats exposed to low-dose LPS (0.1 mg/kg). (**c**) Rats exposed to high-dose LPS (1 mg/kg). In two rats (*leftmost* images in the row), periventricular enhancement is obvious. (**d**) Rats exposed to hypobaric hypoxia (1/2 atm, equivalent to approximately 10 % O_2 at sea level). (**e**) Rats exposed to normobaric hypoxia with 8 % O_2. Periventricular enhancement was substantial in both rats. Statistical significance was set as $p<0.0005$ using a *Z*-test

fluorescent microscopy. In the future, should this method be adapted for human use, such a threshold will require further validation and identification of an appropriate statistical threshold.

It should be noted that we did not observe significant parenchymal enhancement in hypobaric hypoxia nor in low-dose LPS within the tissue. However, we detected changes in the ventricle indicating that there is increased transfer of contrast agent to the ventricle with this mild perturbation.

Moreover, we detected major disruption in the blood-CSF barrier in normobaric hypoxia and high-dose LPS. This is indicated by the fact that most changes were periventricular. Compared with the BBB, the blood-CSF barrier is relatively leakier as it lacks the same tight junction configuration [18].

Limitations of this study include the use of a conservative threshold value for significance ($p<0.0005$), leading to a high degree of false-negative voxels. However, this allowed for a significant reduction of type 1 errors, thereby strengthening our findings of the affected regions. Also, isoflurane during imaging may have exacerbated damage in hypoxic conditions, where the interaction between hypoxia and isoflurane was lethal in a number of animals. This possible

confounder was minimized by using the same anesthetic in control animals, though future studies may consider exploring different agents. Finally, this proof-of-principle concept requires validation in larger studies.

There are a number of advantages to using the voxel-based analysis method. It is a post-MRI acquisition method that provides high spatial resolution and it does not require specific ROIs, as it can detect enhancement anywhere in a given MR image. The steps to generate a voxel map can be compiled with computer software, so it could easily be applied clinically. Also, Gd is regularly administered to patients undergoing MRIs, so this method could be applied for such scans to highlight areas of BBB disruption.

In this study, we have shown that voxel-based analysis can be used to detect subtle disruptions to the BBB and blood-CSF barrier. We showed that there are changes in both inflammation and hypoxia models that are consistent with disruption of the blood-CSF barrier. Thus, further investigation of periventricular disruption in conditions where hypoxia and inflammation play a role is warranted.

Acknowledgments This work was supported by Alberta-Innovates Health Solutions and the National Science and Engineering Research Council Canada.

Conflict of Interest None.

References

1. Chen B et al (2009) Severe blood-brain barrier disruption and surrounding tissue injury. Stroke 40(12):e666–e674
2. Hom J et al (2011) Blood-brain barrier permeability assessed by perfusion CT predicts symptomatic hemorrhagic transformation and malignant edema in acute ischemic stroke. AJNR Am J Neuroradiol 32(1):41–48
3. Oby E, Janigro D (2006) The blood-brain barrier and epilepsy. Epilepsia 47(11):1761–1774
4. Seiffert E et al (2004) Lasting blood-brain barrier disruption induces epileptic focus in the rat somatosensory cortex. J Neurosci 24(36):7829–7836
5. Kumar AJ et al (2000) Malignant gliomas: MR imaging spectrum of radiation therapy- and chemotherapy-induced necrosis of the brain after treatment. Radiology 217(2):377–384
6. Broadwell RD, Sofroniew MV (1993) Serum proteins bypass the blood-brain fluid barriers for extracellular entry to the central nervous system. Exp Neurol 120(2):245–263
7. Fujioka M et al (1999) Novel brain ischemic change on MRI. Delayed ischemic hyperintensity on T1-weighted images and selective neuronal death in the caudoputamen of rats after brief focal ischemia. Stroke 30(5):1043–1046
8. Moseley ME et al (1990) Early detection of regional cerebral ischemia in cats: comparison of diffusion- and T2-weighted MRI and spectroscopy. Magn Reson Med 14(2):330–346
9. Habgood MD et al (2007) Changes in blood-brain barrier permeability to large and small molecules following traumatic brain injury in mice. Eur J Neurosci 25(1):231–238
10. Schneider G et al (2002) Pathophysiological changes after traumatic brain injury: comparison of two experimental animal models by means of MRI. MAGMA 14(3):233–241
11. Provenzale JM, Mukundan S, Dewhirst M (2005) The role of blood-brain barrier permeability in brain tumor imaging and therapeutics. AJR Am J Roentgenol 185(3):763–767
12. Kaya M, Ahishali B (2011) Assessment of permeability in barrier type of endothelium in brain using tracers: Evans blue, sodium fluorescein, and horseradish peroxidase. Methods Mol Biol 763:369–382
13. Soon D et al (2007) Quantification of subtle blood-brain barrier disruption in non-enhancing lesions in multiple sclerosis: a study of disease and lesion subtypes. Mult Scler 13(7):884–894
14. Natah SS et al (2009) Effects of acute hypoxia and hyperthermia on the permeability of the blood-brain barrier in adult rats. J Appl Physiol 107(4):1348–1356
15. Nag S, Picard P, Stewart DJ (2001) Expression of nitric oxide synthases and nitrotyrosine during blood-brain barrier breakdown and repair after cold injury. Lab Invest 81(1):41–49
16. Singh AK, Jiang Y (2004) How does peripheral lipopolysaccharide induce gene expression in the brain of rats? Toxicology 201(1–3):197–207
17. Mikulis DJ, Roberts TP (2007) Neuro MR: protocols. J Magn Reson Imaging 26(4):838–847
18. Redzic Z (2011) Molecular biology of the blood-brain and the blood-cerebrospinal fluid barriers: similarities and differences. Fluids Barriers CNS 8(1):3